ACS Energy LETTERS

http://pubs.acs.org/journal/aelccp

Letter

Lithium−Carbon Composite Anodes for Solid-State Lithium Metal Batteries

Ruixin Wu, Ruihao Deng, Cauê Nogueira, Ru Xiao, Keng Xu, Xin Xu, and Fudong Han*

Cite This: https://doi.org/10.1021/acsenergylett.5c04190

Read Online

ACCESS | Metrics & More | Article Recommendations | Supporting Information

ABSTRACT: While various carbon materials have been reported to make composite lithium metal anodes (LMAs) for liquid-electrolyte batteries, transferring the success to solid-state batteries has proven challenging. Here, we investigate the Li cycling performance of composite LMAs with four representative carbon materials, including carbon black, carbon nanotubes, ordered mesoporous carbon, and graphite. While most carbon materials can demonstrate comparable or better performance than planar Li foil, graphite exhibits the best electrochemical performance in terms of Li cycling. An almost 2-fold increase in the critical current density can be achieved at room temperature after the incorporation of graphite in Li metals due to improvement in the interfacial contact between the anode and the solid electrolyte during Li stripping. The results suggest the effective role of graphite over other types of carbon materials in improving the transport of Li atoms in composite Li anodes for solid-state battery applications.

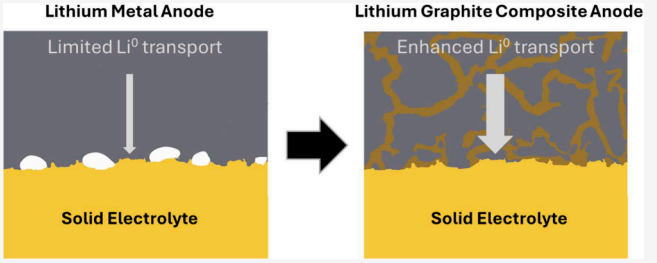

The utilization of high-capacity lithium metal anodes (LMAs) in solid-state batteries is not only desired but also necessary to achieve a competitive energy density with today's lithium-ion batteries (LMAs).[1−6] Despite great success in using LMA for LiPON-based thin film batteries,[7−9] the integration of LMAs in bulk-type solid-state batteries has proven difficult due to the challenges in regulating plating/stripping of thick Li (e.g., ∼25 μm thick at 5 mAh/cm^2) in a controlled manner.[2,10−16] Although the charge transfer kinetics at the Li/solid electrolyte interface seems to be sufficiently fast for practical applications,[2,15−18] recent works show that the diffusion of lithium in the lithium metal during anodic load is limited,[20−25] i.e., the transport of Li in parent metal electrodes is not fast enough to fill the vacancies generated during Li stripping, leading to formation of voids at the Li/solid electrolyte interface. The void formation will then lead to contact loss and unwanted local current hot spots at the interface, which, during the subsequent plating process, can promote dendrite penetration.[13,26,27]

Enhancing the transport of Li in the parent metal electrode is therefore important to address this critical challenge. One promising approach is to introduce Li compounds that have higher Li diffusivity to make a composite Li metal anode.[10,28,29] A recent study from Krauskopf et al. also confirmed that 10 at. % of Mg addition in lithium metal can enhance the Li diffusion coefficient by a factor of 3 to 2.3 × 10^{-11} cm^2/s, leading to effective mitigation of void formation at the Li/solid electrolyte interface.[20] $Li_{13}In_3$ alloy was also used as a host material for Li metal to improve the transport of Li in the anode for solid-state battery applications.[19] Based on a computational study, the author reports a 100-times-faster diffusion of Li atoms on $Li_{13}In_3$ than that of Li.[19] In addition to alloys, carbon was also used as an additive for composite Li metal anodes.[30,31] When lithiated, carbon will be converted to a mixed ionic and electronic conductor with a stable interface with Li metal. Because of the lower density of carbon than typical alloys, the impact on the overall capacity of the anode is much lower than that of alloy-based composite anodes. Yu et al. reported that adding 5 wt % carbon black in Li metal can effectively suppress the pitting formation on Li metal anodes.[30] Significant improvements in Li stripping capacity to 20 mAh/cm^2 under zero stack pressure were also demonstrated in composite Li metal anodes with carbon nanotube additives.[21] Recent works also demonstrated that the introduction of graphite in the composite Li metal anode can improve the Li cycling stability in solid-state batteries.[11,32,33] Given the large variety of carbon materials with differences in particle size, pore size and distribution, degree of graphitization, and surface chemistry, it is unclear which type of carbon is optimal for composite Li metal anodes. In addition, despite the performance improvements in Li cycling, the underlying mechanism for improving Li transport in the composite anodes may not be solely related to the enhancements in Li diffusion in the bulk electrodes. A recent study from Li et al.[34] suggests that the

Received: December 17, 2025
Revised: January 25, 2026
Accepted: February 10, 2026

high diffusivity of Li atoms along the interface between Li and the mixed ionic and electronic conductors, such as lithium alloys and LiC_6, can lead to diffusive creep (i.e., Coble creep) of Li atoms at the interfaces, providing another transport mechanism of Li in addition to bulk diffusion. Li et al. also mentioned that the interfacial diffusivity of Li atoms with typical mixed conductors is so high that the role of the bulk diffusivity of Li atoms is minimal.[34] Understanding the dominant Li transport mechanism in composite Li metal anodes (bulk versus interface transport) is critical for establishing the design principle of high-performance lithium anodes for solid-state batteries, but such information has not been revealed.

In this study, we aim to understand the effect of carbon materials on the Li cycling performance of composite Li metal anodes in solid-state batteries. Four representative carbon materials, including carbon nanotubes (CNTs), carbon black (Super P), mesoporous carbon (CMK-3), and graphite (KS_6), are studied here. The variation of carbon materials, upon lithiation, can not only lead to distinct differences in the Li diffusivities in the bulk[35−37] but also generate different contents of interfaces with Li metal that can promote interfacial creep. By correlating the electrochemical performance with the transport mechanism, we can indirectly probe the Li transport mechanism in these composite anodes. While most carbon materials can demonstrate a comparable or better performance than planar Li foil, graphite exhibits the best electrochemical performance in terms of mitigating void formation and dendrite penetration, suggesting the effective role of graphite over other types of carbon materials in improving the transport of Li atoms in solid-state composite Li metal anodes.

Four representative carbons were selected as the 3D host for this study, including carbon nanotubes (CNTs, length 2.5−20 μm, diameter 6−13 nm), ordered mesoporous carbon (CMK-3, particle size ∼1 μm, pore size 3.8−4.2 nm), carbon black (Super P, particle size ∼40 nm), and graphite (KS_6, particle size ∼3.4 μm) (Table S1). The geometric parameters of these carbons were also confirmed by the SEM tests (Figure S1). Typical features of carbonaceous materials, including the D band and G band, can be seen from the Raman spectra (Figure 1a). By comparing the ratio of the integrated intensity (peak area) of the D band and G band, we can see that the degree of graphitization increases from carbon nanotubes, carbon black, ordered mesoporous carbon, to graphite. The XRD patterns of these carbons (Figure 1b) are also consistent with the previous report.[38−41] A sharp peak corresponding to (002) can be observed for graphite, and the intensity of this peak gradually decreases from CNTs, to carbon black, to mesoporous carbon due to the decrease in the degree of graphitization as well as the size effect.

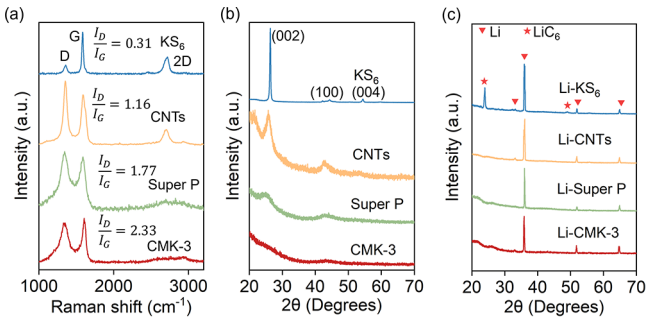

Figure 1. Characterization of carbon host materials. (a) Raman spectra of different types of carbon. (b) XRD pattern of different types of carbon. (c) XRD pattern of different types of Li−C composite anodes.

These carbons were then mixed with a stabilized lithium metal powder (SLMP) to prepare the Li−C composite anode. The composite anode powders were pressed under 15 MPa during cell fabrication as the anodes of solid-state batteries. The content of carbon was fixed at 5 wt % to get a fair comparison across all composite Li anodes.[30] The composite Li anodes are quite dense with a uniform distribution of carbon based on the cross-section SEM images and elemental mapping (Figure S2). Figure 1c shows the XRD results of the composite Li anodes with various carbon additives. All composite anodes exhibit clear reflections from Li metal, but only Li-KS_6 exhibits apparent diffraction patterns from LiC_6.[33,42] The almost-identical XRD patterns of three Li-KS_6 synthesized under the same conditions (Figure S3) also validated the reproducibility of the synthesis method.

The electrochemical performance of various Li−C composite anodes was evaluated by galvanostatic cycling of symmetric cells at increasing current density at room temperature under a stack pressure of 15 MPa (Figures 2a to 2e). Li_6PS_5Cl was used as the solid electrolyte for all of the anodes. The critical current density (CCD), at which a large voltage drop is observed, is used as the parameter to compare the Li cycling performance of these composite anodes. A decrease in the overpotential for Li cycling can be observed after introduction of a carbon additive in Li (Figure S4), suggesting the positive influence of the carbon additive on the kinetics. Figure 2f summarizes the CCD of the anodes with the error bars determined from three repeated measurements (Figure S5). All composite Li anodes except for Li-CMK-3 exhibit higher CCD than pure Li, and Li-KS_6 delivers the highest CCD of 1.1 mA/cm^2, which is roughly a 2× increase compared with bare Li. It should be noted that no apparent differences in the CCD can be observed for the bare Li foil and the Li electrode prepared by pressing the stabilized lithium metal powder (SLMP) (Figure S6). The same trend was also observed for the CCD tested at a lower stack pressure of 5 MPa (Figure S7). The result of the addition of carbon can effectively improve the Li cycling performance of Li anodes, and graphite seems to be the optimal additive.

To understand the effects of various carbons on mitigating void formation at the interface between the Li metal anode and solid electrolytes, we compared the morphological evolution of the anode surface after stripping 2 mAh/cm^2 of Li at 0.5 mA/cm^2 at room temperature, as shown in Figure 3. SEM observations were carried out on the surface of Li peeled off from the solid electrolyte after stripping. No additional electrolyte removal, cleaning, and mechanical separation steps were involved. A relatively smooth surface can be observed for the composite Li metal anode with various carbon additives. An apparent increase in the surface roughness can be observed for bare Li (Figures 3a and 3b) and composite anodes with Super P (Figures 3c and 3d), CMK-3 (Figures 3e and 3f), and CNTs (Figures 3g and 3h) as the additive, suggesting void formation at the Li/solid electrolyte interface under the experimental conditions studied in this work. The void formation seems to be more apparent in the Li-CMK-3 anode, consistent with its lowest CCD in Figure 2. However, the Li-KS_6 composite anode shows a quite smooth surface after stripping (Figures 3i and 3j). To further validate the

https://doi.org/10.1021/acsenergylett.5c04190
ACS Energy Lett. XXXX, XXX, XXX−XXX

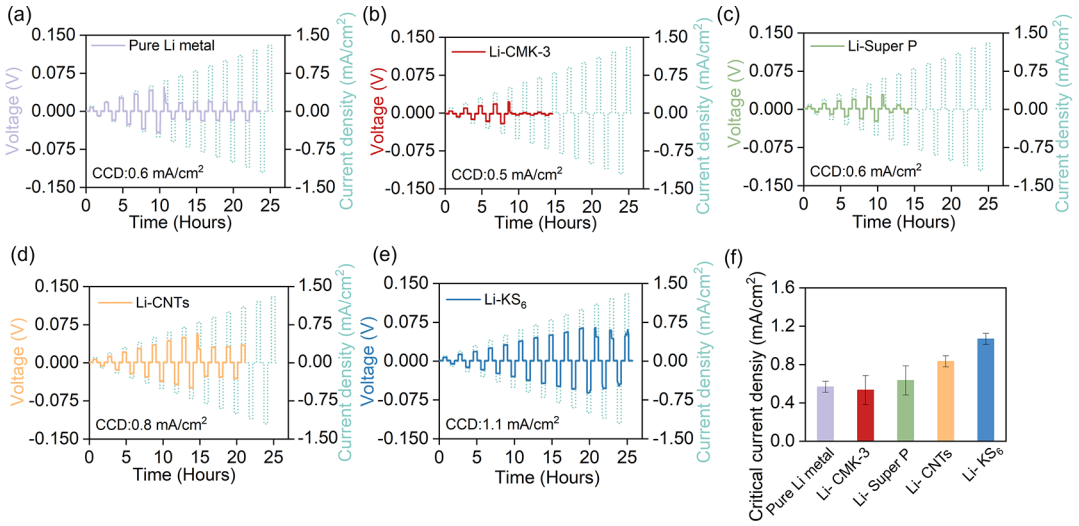

Figure 2. Critical current density of (a) Li, (b) Li-CMK-3, (c) Li-Super P, (d) Li-CNT, and (e) Li-KS_6 anodes tested by Li cycling in a symmetric cell with Li_6PS_5Cl solid electrolyte at room temperature. (f) Comparison of the critical current density of various Li−C composite anodes.

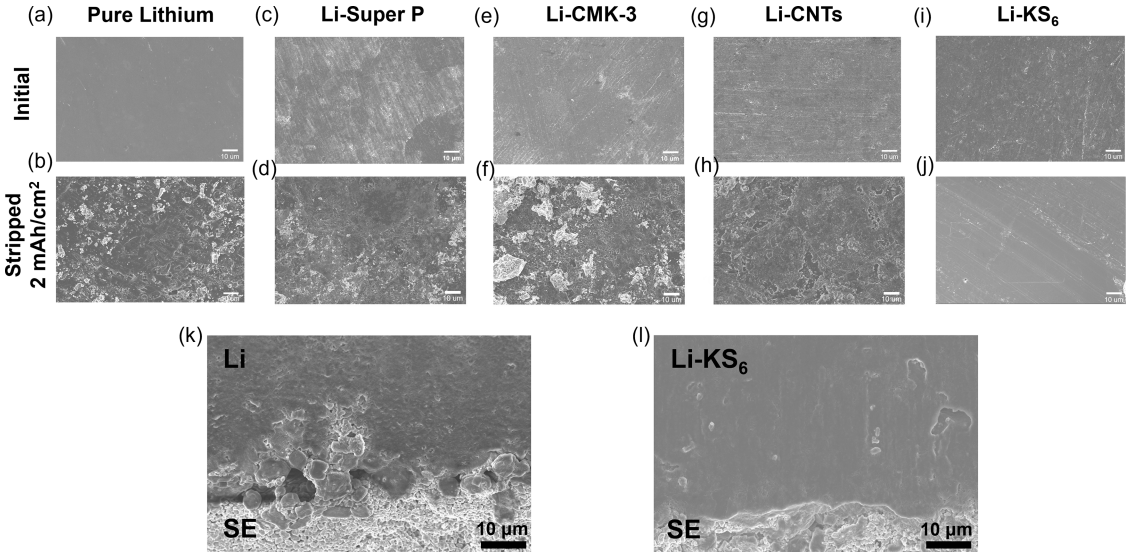

Figure 3. Morphological evolution on the surface of various Li anodes, including bare Li (a and b), Li-Super P (c and d), Li-CMK-3 (e and f), Li-CNTs (g and h), and Li-KS_6 (i and j) before and after stripping 2 mAh/cm^2 Li at 0.5 mA/cm^2 at room temperature. Cross-section SEM image showing the interfacial contact between bare Li (k) and Li-KS_6 (l) and the solid electrolyte after stripping 2 mAh/cm^2 Li at 0.5 mA/cm^2 at room temperature.

morphological evolution of the interface, we also did a cross-sectional SEM image at the Li/electrolyte interface for the bare Li (Figure 3k) and Li-KS_6 (Figure 3l). Apparent void formation can be observed at the interface for bare Li but not for Li-KS_6, further validating the effective mitigation of morphological instability of the composite Li metal anode during stripping.

To understand more about the evolution of interfacial resistance during Li stripping, we investigated the impedance evolution during stripping at a stack pressure of 5 and 15 MPa (Figure 4). The EIS was measured after stripping every 0.5 mAh/cm^2 at a current density of 0.5 mA/cm^2 at room temperature (Figure S8). Figures 4a and 4b show the voltage curve during the stripping test at 5 MPa, and the voltage drop every 1 h is due to the resting period prior to the EIS test. A larger overpotential increase can be observed for the bare Li metal anode compared to the Li-KS_6 composite anode. The overpotential increase is a typical feature of void formation at the Li/electrolyte interface,[20,33,43,44] and the result is also consistent with the increase in the anode/electrolyte interface in the impedance plots (Figure S8). To assist in the visualization of the impedance evolution, we also calculated the distribution of relaxation time (DRT)[45] based on the impedance plot. As the DRT analysis does not require an established equivalent circuit model, it can provide complementary information compared with Nyquist plots.

Figures 4c and 4d show the DRT of the cell with a bare Li metal anode and a Li-KS_6 composite Li anode. As time constant τ is defined as $\tau = RC$, peaks in the DRT in specific time constant ranges can be interpreted to represent electrochemical processes within the cell. Peak identification of the DRT results is based on comparing the EIS and DRT with those of the Li−In/Li_6PS_5Cl/Li−In reference cell (Figure S9), from which the time constant (τ) of the ionic transport in

https://doi.org/10.1021/acsenergylett.5c04190
ACS Energy Lett. XXXX, XXX, XXX−XXX

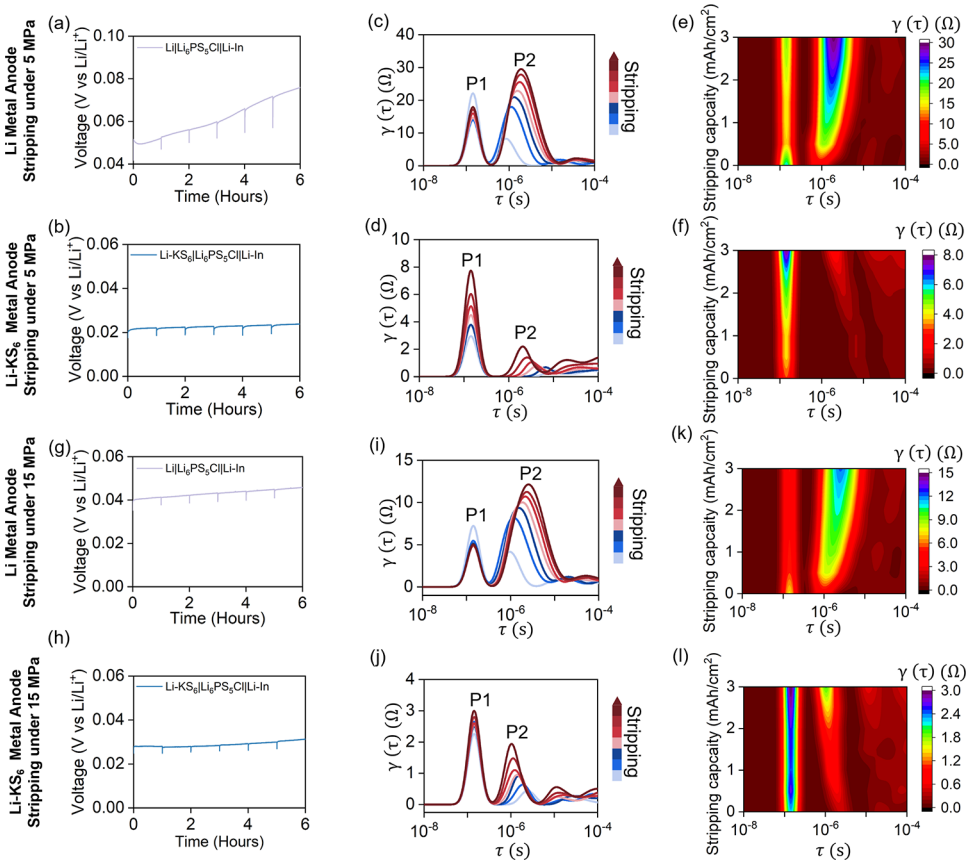

Figure 4. Voltage profiles during the Li stripping of the bare Li anode (a) and Li-KS_6 composite anode (b) at a stack pressure of 5 MPa. DRT evolution and corresponding 2D DRT surface during Li stripping of the bare Li anode (c and e) and Li-KS_6 composite anode (d and f) at a stack pressure of 5 MPa. (a) Voltage profiles during the Li stripping of the bare Li anode (g) and Li-KS_6 composite anode (h) at a stack pressure of 15 MPa. DRT evolution and corresponding 2D DRT surface during Li stripping of the bare Li anode (i and k) and Li-KS_6 composite anode (j and l) at a stack pressure of 15 MPa. The EIS was measured after stripping every 0.5 mAh/cm^2 at a current density of 0.5 mA/cm^2 at room temperature. $Li_{0.5}In$ was used as the cathode and Li_6PS_5Cl was used as the solid electrolyte for the stripping test.

the Li_6PS_5Cl solid electrolyte is determined to be at 10^{-7} s, while the interfacial resistance between Li−In and the solid electrolyte is negligible. Therefore, the remaining peak P2 with a time constant of around 10^{-6} s is attributed to the Li−electrolyte interfacial processes (Figures 4c and 4d). The evolution of this interfacial resistance of this peak can indirectly reflect the interfacial contact between the Li and the solid electrolyte, assuming the SEI resistance is constant due to the relatively good stability of Li_6PS_5Cl.[46] As shown in the 2D DRT results (Figures 4e and 4f), while the resistance for peak P2 for bare Li and Li-KS_6 composite anodes both increased, a much larger increase can be observed for the bare Li anode. Moreover, the dramatic increase in interfacial resistance occurs at a much smaller stripping capacity (0.5 mAh/cm^2) for the bare Li metal. Increasing the stack pressure to 15 MPa helps to reduce the overpotential increase of the bare Li anode during stripping (Figure 4g), due to the enhanced plastic deformation of Li. A larger overpotential increase (Figures 4g and 4h) and a larger resistance of peak P2 (Figures 4i to 4l) can still be observed for the bare Li anode when compared with the Li-KS_6 composite anode. Given that the increase in interfacial resistance is largely related to contact loss, the impedance analysis further validates the effect of the KS_6 additive in mitigation of the void formation at the Li/electrolyte interface during stripping.

Figures 5a to 5d show the voltage profiles during galvanostatic cycling of Li|Li_6PS_5Cl|Li and Li-KS6|Li_6PS_5Cl|Li-KS_6 cells at 0.2 mA/cm^2 and 0.2 mAh/cm^2 at room temperature. An apparent voltage drop, due to dendrite penetration, can be observed for the cell with a bare Li metal anode after 420 h Li cycling (Figure 5b), while the Li-KS_6|Li_6PS_5Cl|Li-KS_6 cell can be cycled for more than 2500 h without signs of shorting (Figure 5d). The excellent performance of Li-KS_6 in dendrite suppression was also demonstrated in solid-state full cells with the $LiCoO_2$ cathode (Figures 5e and 5f). The Li|Li_6PS_5Cl|$LiCoO_2$ cell shorted during charging at 1.0 C (Figure 5e), while the Li-KS_6|Li_6PS_5Cl|$LiCoO_2$ cell can be charged/discharged at 2.0 C without shorting (Figure 5f). The excellent stability of Li-KS_6 was also demonstrated from the cycling test of the Li-KS_6|Li_6PS_5Cl|$LiCoO_2$ full cell at 1C at room temperature, and no shorting can be observed for 100 cycles (Figure S10). The electrochemical performance of the Li-KS_6 composite anode in the Li−Li symmetrical cells and full cells is much higher than other composite Li anodes reported in the literature (Table S2).[11,17,32,33,47,48]

The findings from this work indicate that the introduction of graphite into Li metal can help mitigate the void formation at the interface. As void formation during stripping is largely governed by the diffusion limit of Li atoms in the Li anode,[20] the superior performance of the composite Li anode with graphite additive also implies enhanced transport of Li atoms

https://doi.org/10.1021/acsenergylett.5c04190
ACS Energy Lett. XXXX, XXX, XXX−XXX

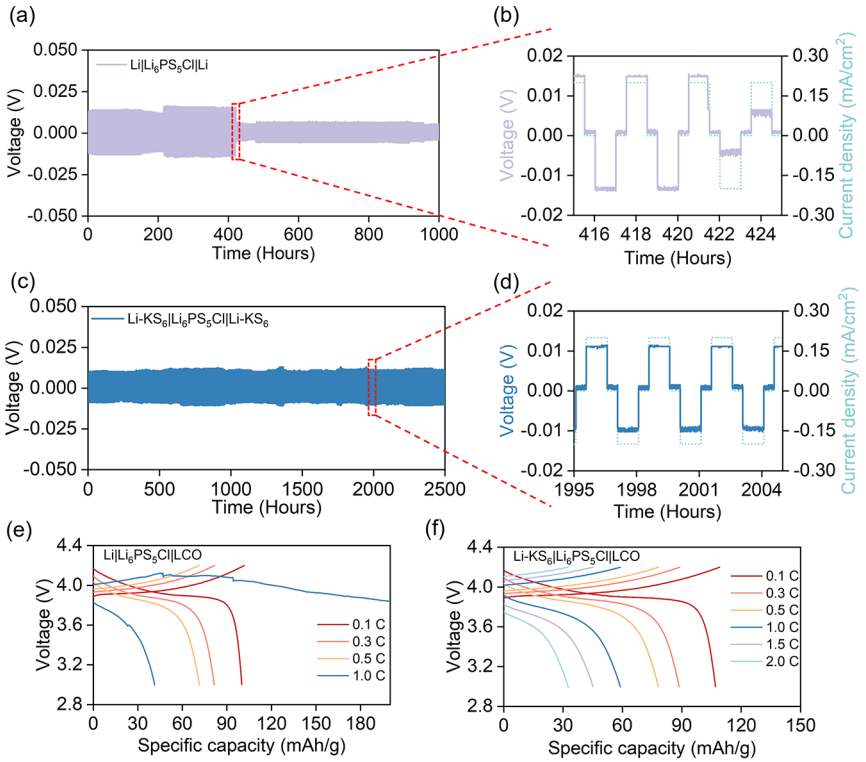

Figure 5. Galvanostatic cycling of (a) Li|Li_6PS_5Cl|Li and (c) Li-KS_6|Li_6PS_5Cl|Li-KS_6 at 0.2 mA/cm^2 and 0.2 mAh/cm^2. (b) and (d) show the enlarged voltage profiles of Li|Li_6PS_5Cl|Li cells. Charge/discharge curves of Li|Li_6PS_5Cl|$LiCoO_2$ (e) and Li-KS_6|Li_6PS_5Cl|$LiCoO_2$ (f). All tests were performed at room temperature.

in the composite Li anodes, although the exact mechanism for such enhancements remains elusive. In addition to the large content of LiC_6, microstructural features should also play a role, depending on the exact transport property of Li atoms of LiC_6 on the surface versus in the bulk. It should be noted that the transport mechanism and transport property of carbonaceous materials are not well understood.[44] For example, it is still unclear how Li was transported through the carbon interlayer that has been widely used in anode-free solid-state batteries.[49−51] In addition to bulk diffusion of Li ions in the lithiated carbon, surface transport of Li ions[52] and interfacial transport of Li atoms (through creeping)[34] may also play an important role. We also highlight the different requirements in the transport property of carbon as an interlayer for an anode-free cell and as an additive for a composite Li metal anode. Because of the low content of carbon additive in the composite Li anode (~5 wt % in this work), the transport in the composite Li anodes is governed by diffusion of lithium atoms. As a result, the carbon material used as an interlayer may not work well as an additive in a composite Li anode. It should also be noted that further increase in the carbon content to 15 wt % does not necessarily lead to enhancement in CCD (Figure S11), probably due to variation in the mechanical property of the composite anodes (Figure S12).[21] The change in the mechanical properties of the composite Li anode at a higher graphite content leads to challenges in maintaining interfacial contact at the same stack pressure. While the interfacial chemistry between the Li_6PS_5Cl solid electrolyte and various carbon composite anodes can be different depending on the interfacial contact area as well as the electronic conductivity of the carbon, we do not see a direct correlation between the interphase resistance, which can be reflected from the overpotential at lower current densities of the CCD tests (Figure S4), and the CCD of the Li−C composite anodes. Further work is still needed to integrate the mechanical properties with the transport properties to develop advanced composite Li metal anodes for solid-state batteries.

In summary, we studied the effect of the carbon material on the electrochemical performance of Li−C composite Li metal anodes. Four representative carbon materials, including carbon black, carbon nanotubes, mesoporous carbon, and graphite, were used to make a Li−C composite. The incorporation of 5 wt % carbon materials can generally enhance the dendrite suppression capability of the composite anodes, with the Li−graphite composite anode delivering the highest improvement in the critical current density (1.1 mA/cm^2 vs 0.6 mA/cm^2 for the bare Li anode). Combining SEM and impedance analysis, the effective role of graphite was also attributed to the mitigation of the void formation at the interface between the anode and the solid electrolyte during stripping. The excellent performance of the Li−graphite composite anode enabled stable Li cycling for >2500 h at 0.2 mA/cm^2 and 0.2 mAh/cm^2 at room temperature and enabled a $LiCoO_2$-based solid-state full cell that can be charged at a high rate of 2C at room temperature. Since void formation during stripping is largely governed by the diffusion limit of Li atoms in the Li anode, the superior performance of the Li−graphite composite anode also implies enhanced transport of Li atoms in the graphite-based composite Li anodes. This work provides insights into establishing the design principles of Li−metal anodes for solid-state batteries.

https://doi.org/10.1021/acsenergylett.5c04190
ACS Energy Lett. XXXX, XXX, XXX−XXX

EXPERIMENTAL SECTION

Materials Synthesis

Lithium−carbon composite anodes were prepared by a mechanical ball milling method. Carbon black (Super P, MTI), carbon nanotubes (CNTs, Sigma-Aldrich), mesoporous carbon (CMK-3, ACS Material LLC), and graphite (KS_6, MSE Supplies) were ball-milled with stabilized lithium metal powder (SLMP, FMC). For the milling process, the powders were weighed and mixed in a 50 mL stainless-steel jar (Retsch) in the glovebox. The jar was sealed by a safety closure device (Retsch), transferred out of the glovebox, and milled at 100 rpm for 1 h using a planetary ball mill (Retsch PM100). After being milled, the jar was then transferred into the glovebox to collect the sample. The content of carbon is 5 wt % in the composite Li metal anodes. The $Li_{0.5}In$ alloy anode was prepared by shaking a stoichiometric amount of the SLMP powder and indium powder (99.99%, Sigma-Aldrich) utilizing a vortex mixer (VX-200, VWR) for 30 min. The $LiCoO_2$ composite cathode was prepared by ball milling $LiNbO_3$-coated $LiCoO_2$ cathode powder and Li_6PS_5Cl solid electrolyte with a weight ratio of 60:40 in a 50 mL stainless steel jar at 100 rpm for 1 h.

Material Characterization

A Carl Zeiss Supra 55 FESEM instrument was used to investigate the morphology evolution. The energy dispersive spectrometry (EDS) mapping test was performed using VERSA 3D SEM equipment. A cross-section sample was prepared by soaking the samples in liquid nitrogen (LN) for 1 min and then cutting with a blade. The X-ray diffraction test was performed using a PanAlytical X'Pert diffractometer with a copper irradiation source (Cu Ka $^1/_4$ 0.1540, 6 nm). Raman spectra were acquired using a Witec Alpha 300 RA+ Raman/AFM system equipped with a 532 nm excitation laser and a spatial resolution of approximately 1 μm. A 50× objective lens was employed to focus the laser on the sample. The laser power in the sample was maintained at 0.5 mW to minimize local heating. Spectra were collected using a 600 g/mm grating centered at 1900 cm^{-1}, with 50 accumulations and an exposure time of 10 s each. The uniaxial compression test was performed with an Instron 4204 at a strain rate of 0.1 mm/min.

Cell Fabrication

To fabricate the Li/Li symmetrical cell with various anodes, 100 mg of Li_6PS_5Cl solid electrolyte (NEI) was placed into a 10 mm diameter polyaryl ether ether ketone (PEEK) cylinder and cold-pressed for 2 min under 300 MPa. Then, 15 mg of lithium carbon composite anode was placed on both sides under 15 MPa. To fabricate the solid-state full cell with a $LiCoO_2$ cathode and Li_6PS_5Cl solid electrolyte, 80 mg of Li_6PS_5Cl was placed into a PEEK cylinder and cold-pressed for 2 min under 300 MPa. Then 5 mg of cathode composite powder was dispersed on one side of the PEEK cylinder and cold-pressed for 2 min at 350 MPa. After that, 15 mg of Li−C composite anode was placed on the other side under a stack pressure of 15 MPa. The stack pressure of the cell was measured by using a load sensor during cell fabrication. After the target pressure was reached, the pressure was fixed using four screws in the cell housing. No real-time pressure adjustments were applied to maintain the stack pressure during the measurement. All cells were tested at room temperature. All the experiments were performed in an argon glovebox (H_2O < 0.5 ppm, O_2 < 0.5 ppm).

Electrochemical Measurements

The galvanostatic charge/discharge tests were performed under room temperature using a LAND battery tester (Wuhan LAND Electronics Co., Ltd.). For the CCD test, it was tested from 0.1 mA/cm^2 with a current increment of 0.1 mA/cm^2 every 30 min until the short-circuit happened. Electrochemical impedance spectroscopy (EIS) during stripping was tested using a potentiostat (Biologic VSP-300). The frequency range for the EIS measurement is 7 MHz to 1 Hz with a perturbation voltage of 10 mV. All electrochemical measurements were performed at room temperature.

ASSOCIATED CONTENT

Supporting Information

The Supporting Information is available free of charge at https://pubs.acs.org/doi/10.1021/acsenergylett.5c04190.

Morphology and characteristic properties of carbons; cross-section and EDS of the Li-C composite anode; XRD of Li-KS_6 composite anodes; voltage profiles for all carbons during the CCD test; CCD measurements of composite Li anodes; CCD of SLMP anodes; CCD of composite anodes under 5 MPa; evolution of EIS during stripping; EIS and DRT of Li-In|Li_6PS_5Cl|Li−In symmetry cells; cycling performance of the Li-KS_6|Li_6PS_5Cl|$LiCoO_2$ cell; summary of electrochemical performances of all-solid-state batteries with a carbon-containing composite Li metal anode; CCD of composite anodes with 15 wt % carbon contents; strain−stress test of Li and Li-KS_6 (PDF)

AUTHOR INFORMATION

Corresponding Author

Fudong Han − *Department of Mechanical, Aerospace and Nuclear Engineering, Rensselaer Polytechnic Institute, Troy, New York 12180, United States;* orcid.org/0000-0003-2507-4340; Email: hanf2@rpi.edu

Authors

Ruixin Wu − *Department of Mechanical, Aerospace and Nuclear Engineering, Rensselaer Polytechnic Institute, Troy, New York 12180, United States*

Ruihao Deng − *Department of Mechanical, Aerospace and Nuclear Engineering, Rensselaer Polytechnic Institute, Troy, New York 12180, United States*

Cauê Nogueira − *School for Engineering of Matter, Transport, and Energy, Arizona State University, Tempe, Arizona 85287, United States*

Ru Xiao − *Department of Mechanical, Aerospace and Nuclear Engineering, Rensselaer Polytechnic Institute, Troy, New York 12180, United States*

Keng Xu − *Department of Mechanical, Aerospace and Nuclear Engineering, Rensselaer Polytechnic Institute, Troy, New York 12180, United States*

Xin Xu − *The Polytechnic School, Arizona State University, Mesa, Arizona 85212, United States*

Complete contact information is available at: https://pubs.acs.org/10.1021/acsenergylett.5c04190

https://doi.org/10.1021/acsenergylett.5c04190
ACS Energy Lett. XXXX, XXX, XXX−XXX

Author Contributions

R. Wu contributed to the experiments, characterizations, data analysis, and manuscript writing. R. Deng contributed to the characterization. R. Xiao and K. Xu contributed to the data analysis. X. Xu and C. Nogueira performed the Raman measurement. All authors discussed the results. F. Han supervised the project and edited the manuscript.

Notes

The authors declare no competing financial interest.

■ ACKNOWLEDGMENTS

The authors acknowledge support from the U.S. National Science Foundation (Award No. DMR-2223217) and the U.S. Department of Energy (DOE), Advanced Research Projects Agency for Energy (ARPA-E), IGNIITE program (Award No. DE-AR0001927).

■ REFERENCES

(1) Janek, J.; Zeier, W. G. A Solid Future for Battery Development. *Nature Energy 1*, 9 (**2016**): 1−4.
(2) Krauskopf, T.; Richter, F. H.; Zeier, W. G.; Janek, J. Physicochemical Concepts of the Lithium Metal Anode in Solid-State Batteries. *Chem. Rev. 120*, 15 (**2020**): 7745−7794.
(3) Alexander, G. V.; Shi, C.; O'Neill, J.; Wachsman, E. D. Extreme Lithium-Metal Cycling Enabled by a Mixed Ion- and Electron-Conducting Garnet Three-Dimensional Architecture. *Nat. Mater. 22*, 9 (**2023**): 1136−1143.
(4) Fuller, S. T.; Huang, Y.; Wu, R.; Han, F.; Kent Zheng, J. X.; Vasiljevic, N. Engineering Electrodeposition for Next-Generation Batteries. *Electrochemical Society Interface 33*, 2 (**2024**): 55.
(5) Fang, C.; Li, J.; Zhang, M.; Zhang, Y.; Yang, F.; Lee, J. Z.; Lee, M.-H.; Alvarado, J.; Schroeder, M. A.; Yang, Y.; et al.Quantifying Inactive Lithium in Lithium Metal Batteries. *Nature 572*, 7770 (**2019**): 511−515.
(6) Fang, C.; Wang, X.; Meng, Y. S. Key Issues Hindering a Practical Lithium-Metal Anode. *Trends in Chemistry* **2019**, *1* (2), 152−158.
(7) Neudecker, B. J.; Dudney, N. J.; Bates, J. B. "Lithium-Free" Thin-Film Battery with In Situ Plated Li Anode. *J. Electrochem. Soc.* **2000**, *147* (2), 517.
(8) Huang, Y.; Zhang, Y.; Wu, R.; Shao, B.; Deng, R.; Das, R.; Han, F. Hydride-Based Interlayer for Solid-State Anode-Free Battery. *ACS Energy Letters* **2024**, *9* (7), 3409−3417.
(9) Li, S.-Y.; Wang, W.-P.; Xin, S.; Zhang, J.; Guo, Y.-G. A Facile Strategy to Reconcile 3D Anodes and Ceramic Electrolytes for Stable Solid-State Li Metal Batteries. *Energy Storage Materials* **2020**, *32*, 458−464.
(10) Kerman, K.; Luntz, A.; Viswanathan, V.; Chiang, Y.-M.; Chen, Z. Review—Practical Challenges Hindering the Development of Solid State Li Ion Batteries. *J. Electrochem. Soc.* **2017**, *164* (7), A1731.
(11) Duan, J.; Wu, W.; Nolan, A. M.; Wang, T.; Wen, J.; Hu, C.; Mo, Y.; Luo, W.; Huang, Y. Lithium−Graphite Paste: An Interface Compatible Anode for Solid-State Batteries. *Adv. Mater.* **2019**, *31* (10), 1807243.
(12) Haslam, C. G.; Fuchs, T.; Liao, D. W.; Becker, J.; Dasgupta, N. P.; Janek, J.; Sakamoto, J. The Effect of Alloying Interlayers on Lithium Anode Morphology and Microstructure in "Anode-Free" Solid-State Batteries. *ACS Energy Letters* **2025**, *10* (5), 2285−2291.
(13) Kasemchainan, J.; Zekoll, S.; Spencer Jolly, D.; Ning, Z.; Hartley, G. O.; Marrow, J.; Bruce, P. G. Critical Stripping Current Leads to Dendrite Formation on Plating in Lithium Anode Solid Electrolyte Cells. *Nat. Mater.* **2019**, *18* (10), 1105−1111.
(14) Sandoval, S. E.; Haslam, C. G.; Vishnugopi, B. S.; Liao, D. W.; Yoon, J. S.; Park, S. H.; Wang, Y.; Mitlin, D.; Hatzell, K. B.; Siegel, D. J.; Mukherjee, P. P.; et al.Electro-Chemo-Mechanics of Anode-Free Solid-State Batteries. *Nat. Mater. 24*, 5 (**2025**): 673−681.
(15) Wang, Y.; Liu, Y.; Nguyen, M.; Cho, J.; Katyal, N.; Vishnugopi, B. S.; Hao, H.; Fang, R.; Wu, N.; Liu, P.et al.Stable Anode-Free All-Solid-State Lithium Battery through Tuned Metal Wetting on the Copper Current Collector. *Adv. Mater. 35*, 8 (**2023**): 2206762.
(16) Wang, Y.; Raj, V.; Naik, K. G.; Vishnugopi, B. S.; Cho, J.; Nguyen, M.; Recker, E. A.; Su, Y.; Celio, H.; Dolocan, A.; et al.Control of Two Solid Electrolyte Interphases at the Negative Electrode of an Anode-Free All Solid-State Battery Based on Argyrodite Electrolyte. *Adv. Mater. 37*, 11 (**2025**): 2410948.
(17) Liang, Z.; Nafis, M. S.; Cho, S.; Guo, F.; Zhou, H.; Guthrey, H.; Lee, S.; Whittingham, M. S.; Ban, C. Pressure-Tolerant 3D Anodes Enable Short-Circuit Prevention and Low Heat Generation in Argyrodite Solid-State Batteries. *ACS Energy Letters* **2025**, *10*, 2461−2467.
(18) Wu, D.; Peng, J.; Jiang, Z.; Zhu, L.; Wu, Y.; Xu, C.; Wang, Z.; Yang, M.; Li, H.; Chen, L.; et al.Low-Pressure Dendrite-Free Sulfide Solid-State Battery with 3D LiSi@Li-Phen-Ether Anode. *Energy Storage Materials 72* (**2024**): 103749.
(19) Gao, X.; Yang, X.; Jiang, M.; Zheng, M.; Zhao, Y.; Li, R.; Ren, W.; Huang, H.; Sun, R.; Wang, J.; et al.Fast Ion Transport in Li-Rich Alloy Anode for High-Energy-Density All Solid-State Lithium Metal Batteries. *Adv. Funct. Mater. 33* (**2023**): 2209715.
(20) Krauskopf, T.; Mogwitz, B.; Rosenbach, C.; Zeier, W. G.; Janek, J. Diffusion Limitation of Lithium Metal and Li−Mg Alloy Anodes on LLZO Type Solid Electrolytes as a Function of Temperature and Pressure. *Adv. Energy Mater.* **2019**, *9*, 1902568.
(21) Fuchs, T.; Haslam, C. G.; Moy, A. C.; Lerch, C.; Krauskopf, T.; Sakamoto, J.; Richter, F. H.; Janek, J. Increasing the Pressure-Free Stripping Capacity of the Lithium Metal Anode in Solid-State-Batteries by Carbon Nanotubes. *Adv. Energy Mater.* **2022**, *12*, 2201125.
(22) Jeon, Y.; Lee, D. J.; Zheng, H.; Behara, S. S.; Lee, J.-P.; Wu, J.; Li, F.; Tang, W.; Zhang, L.; Chen, Y.-T.; et al. Lithium Diffusion-Controlled Li-Al Alloy Negative Electrode for All-Solid-State Battery. *Nat. Commun. 16* (**2025**): 9629.
(23) Mann, M.; Schwab, C.; Dos Santos, L. C. P.; Spatschek, R.; Fattakhova-Rohlfing, D.; Finsterbusch, M. Improving the Rate Performance of Lithium Metal Anodes: In-Situ Formation of 3D Interface Structures by Mechanical Mixing with Sodium Metal. *Energy Storage Materials* **2025**, *74*, No. 103975.
(24) Liao, D. W.; Zeng, D.; Mulla, M.; Madanchi, A.; Kawakami, H.; Aihara, Y.; Aotani, K.; Thouless, M. D.; Dasgupta, N. P. Effects of Interfacial Adhesion on Lithium Plating Location in Solid-State Batteries with Carbon Interlayers. *Adv. Mater.* **2025**, *37*, 2502114.
(25) Fuchs, T.; Haslam, C. G.; Moy, A. C.; Lerch, C.; Krauskopf, T.; Sakamoto, J.; Richter, F. H.; Janek, J. Increasing the Pressure-Free Stripping Capacity of the Lithium Metal Anode in Solid-State-Batteries by Carbon Nanotubes. *Adv. Energy Mater.* **2022**, *12* (26), 2201125.
(26) Avvaru, V. S.; Ogunfunmi, T.; Jeong, S.; Diallo, M. S.; Watt, J.; Scott, M. C.; Kim, H. Tin−Carbon Dual Buffer Layer to Suppress Lithium Dendrite Growth in All-Solid-State Batteries. *ACS Nano* **2025**, *19* (18), 17347−17356.
(27) Liu, H.; Cheng, X.-B.; Huang, J.-Q.; Yuan, H.; Lu, Y.; Yan, C.; Zhu, G.-L.; Xu, R.; Zhao, C.-Z.; Hou, L.-P.; et al. Controlling Dendrite Growth in Solid-State Electrolytes. *ACS Energy Letters 5*, 3 (**2020**): 833−843.
(28) Huang, Y.; Shao, B.; Han, F. Li Alloy Anodes for High-Rate and High-Areal-Capacity Solid-State Batteries. *Journal of Materials Chemistry A* **2022**, *10* (23), 12350−12358.
(29) Wan, H.; Wang, Z.; Zhang, W.; He, X.; Wang, C. Interface Design for All-Solid-State Lithium Batteries. *Nature* **2023**, *623* (7988), 739−744.
(30) Yu, S.; Wang, S.; Miao, Q.; Hui, Z.; Hyun, G.; Holoubek, J.; Yu, X.; Gao, J.; Liu, P. Composite Lithium Metal Structure to Mitigate Pulverization and Enable Long-Life Batteries. *Adv. Energy Mater.* **2023**, *13* (40), 2302400.
(31) He, X.; Zhang, K.; Zhu, Z.; Tong, Z.; Liang, X. 3D-Hosted Lithium Metal Anodes. *Chem. Soc. Rev.* **2024**, *53* (1), 9−24.

https://doi.org/10.1021/acsenergylett.5c04190
ACS Energy Lett. XXXX, XXX, XXX−XXX

(32) Xing, X.; Li, Y.; Wang, S.; Liu, H.; Wu, Z.; Yu, S.; Holoubek, J.; Zhou, H.; Liu, P. *Graphite-Based Lithium-Free 3D Hybrid Anodes for High Energy Density All-Solid-State Batteries. ACS Energy Letters* **2021**, *6*, 1831−1838.
(33) Wang, Z.-X.; Lu, Y.; Zhao, C.-Z.; Huang, W.-Z.; Huang, X.-Y.; Kong, W.-J.; Li, L.-X.; Wang, Z.-Y.; Yuan, H.; Huang, J.-Q.; et al.Suppressing Li Voids in All-Solid-State Lithium Metal Batteries through Li Diffusion Regulation. *Joule 8*, 10 (**2024**): 2794−2810.
(34) Chen, Y.; Wang, Z.; Li, X.; Yao, X.; Wang, C.; Li, Y.; Xue, W.; Yu, D.; Kim, S. Y.; Yang, F.; et al.Li Metal Deposition and Stripping in a Solid-State Battery via Coble Creep. *Nature 578*, 7794 (**2020**): 251−255.
(35) Kaskhedikar, N. A.; Maier, J. Lithium Storage in Carbon Nanostructures. *Adv. Mater.* **2009**, *21* (25−26), 2664−2680.
(36) Persson, K.; Sethuraman, V. A.; Hardwick, L. J.; Hinuma, Y.; Meng, Y. S.; Van Der Ven, A.; Srinivasan, V.; Kostecki, R.; Ceder, G. Lithium Diffusion in Graphitic Carbon. *J. Phys. Chem. Lett. 1*, 8 (**2010**): 1176−1180.
(37) Yu, P.; Popov, B. N.; Ritter, J. A.; White, R. E. Determination of the Lithium Ion Diffusion Coefficient in Graphite. *J. Electrochem. Soc.* **1999**, *146* (1), 8.
(38) Siddarth, R. K.; Manopriya, M.; Swathi, G.; Vijayvenkataraman, G.; Aranganayagam, K. R. One Step Synthesis of Reduced and Moringa Oleifera Treated Graphene Oxide: Characterization and Antibacterial Studies. In *Proceedings of the International Conference on Nanomedicine (ICON-2019)*; Rajan, M., Anand, K., Chuturgoon, A., Eds.; Springer Proceedings in Materials; Springer International Publishing: Cham, 2019; pp 54−62.
(39) Vélez, V.; López, B.; Palacio, R.; Sierra, L. A Novel Mesoporous Carbon as Potential Conductive Additive for a Li-Ion Battery Cathode. *C* **2019**, *5* (4), 81.
(40) Huq, M. M.; Hsieh, C.-T.; Ho, C.-Y. Preparation of Carbon Nanotube-Activated Carbon Hybrid Electrodes by Electrophoretic Deposition for Supercapacitor Applications. *Diamond Relat. Mater.* **2016**, *62*, 58−64.
(41) He, Z.; Zhang, G.; Chen, Y.; Xie, Y.; Zhu, T.; Guo, H.; Chen, Y. The Effect of Activation Methods on the Electrochemical Performance of Ordered Mesoporous Carbon for Supercapacitor Applications. *J. Mater. Sci.* **2017**, *52* (5), 2422−2434.
(42) Sacci, R. L.; Gill, L. W.; Hagaman, E. W.; Dudney, N. J. Operando NMR and XRD Study of Chemically Synthesized LiC Oxidation in a Dry Room Environment. *J. Power Sources* **2015**, *287*, 253−260.
(43) Krauskopf, T.; Hartmann, H.; Zeier, W. G.; Janek, J. Toward a Fundamental Understanding of the Lithium Metal Anode in Solid-State Batteries—An Electrochemo-Mechanical Study on the Garnet-Type Solid Electrolyte $Li_{6.25}Al_{0.25}La_3Zr_2O_{12}$. *ACS Appl. Mater. Interfaces* **2019**, *11* (15), 14463−14477.
(44) Fuchs, T.; Haslam, C. G.; Moy, A. C.; Lerch, C.; Krauskopf, T.; Sakamoto, J.; Richter, F. H.; Janek, J. Increasing the Pressure-Free Stripping Capacity of the Lithium Metal Anode in Solid-State-Batteries by Carbon Nanotubes. *Adv. Energy Mater.* **2022**, *12* (26), 2201125.
(45) Wan, T. H.; Saccoccio, M.; Chen, C.; Ciucci, F. Influence of the Discretization Methods on the Distribution of Relaxation Times Deconvolution: Implementing Radial Basis Functions with DRTtools. *Electrochim. Acta* **2015**, *184*, 483−499.
(46) Wenzel, S.; Sedlmaier, S. J.; Dietrich, C.; Zeier, W. G.; Janek, J. Interfacial Reactivity and Interphase Growth of Argyrodite Solid Electrolytes at Lithium Metal Electrodes. *Solid State Ionics* **2018**, *318*, 102−112.
(47) Park, S. H.; Jun, D.; Lee, G. H.; Lee, S. G.; Jung, J. E.; Bae, K. Y.; Son, S.; Lee, Y. J. Designing 3D Anode Based on Pore-Size-Dependent Li Deposition Behavior for Reversible Li-Free All-Solid-State Batteries. *Advanced Science* **2022**, *9* (28), 2203130.
(48) Liu, J.; Wang, L.; Cheng, Y.; Huang, M.; Zhao, L.; Zheng, C.; Li, W.; Gao, H.; Li, Z.; Wen, Z.; et al.Modulating the Spatio-Temporal Sequence of Lithium Plating and Stripping via a 3D Host for Solid State Batteries. *Adv. Mater. 37*, 20 (**2025**): 2418720.
(49) Lee, Y.-G.; Fujiki, S.; Jung, C.; Suzuki, N.; Yashiro, N.; Omoda, R.; Ko, D.-S.; Shiratsuchi, T.; Sugimoto, T.; Ryu, S.et al.High-Energy Long-Cycling All-Solid-State Lithium Metal Batteries Enabled by Silver−Carbon Composite Anodes. *Nature Energy 5*, 4 (**2020**): 299−308.
(50) Park, S. H.; Naik, K. G.; Vishnugopi, B. S.; Mukherjee, P. P.; Hatzell, K. B. Lithium Kinetics in Ag−C Porous Interlayer in Reservoir-Free Solid-State Batteries. *Adv. Energy Mater.* **2025**, *15* (16), 2405129.
(51) Suzuki, N.; Yashiro, N.; Fujiki, S.; Omoda, R.; Shiratsuchi, T.; Watanabe, T.; Aihara, Y. Highly Cyclable All-Solid-State Battery with Deposition-Type Lithium Metal Anode Based on Thin Carbon Black Layer. *Advanced Energy and Sustainability Research* **2021**, *2* (11), 2100066.
(52) Zhou, J.; Wang, S.; Wu, C.; Qi, J.; Wan, H.; Lai, S.; Ko, T. W.; Liang, Z.; Feng, S.; Zhou, K.; et al.Superionic Surface Li-Ion Transport in Carbonaceous Materials. *Nano Lett. 25*, 34 (**2025**): 12876−12883.

https://doi.org/10.1021/acsenergylett.5c04190
ACS Energy Lett. XXXX, XXX, XXX−XXX